ALMA Cycle-7 Study Project: Close-Out Report

Technology Development of Quantum-Limited, Ultra-Wideband RF Amplifiers for ALMA: A 65-150 GHz Amplifier Test Case

1. Introduction

Traveling-wave kinetic-inductance parametric amplifiers (TKIPs) are a promising new technology to improve the bandwidth and sensitivity of radio astronomical receivers, especially at millimeter/submillimeter-wave frequencies, where the theoretical limits of SIS-based receivers have almost been realized. Therefore, successful development of TKIPs could significantly improve the performance of ALMA and other future radio telescopes. For this reason, the study of TKIPs is considered a strategic investment in NRAO's long-term technology program.

2. Goals

The goals of this study were to:

(1) Characterize the noise, gain, and dynamic range of W-band TKIPs fabricated at JPL.
(2) Develop new materials growth and fabrication techniques at the University of Virginia's "Innovations in Fabrication" (IFAB) laboratory.

3. Unexpected Delays

Several unexpected developments severely impacted the execution of this study, ultimately limiting the scope and causing significant delays. These developments included the loss of the original PI and the Covid pandemic, which delayed hiring a new PI by two years and prevented unfettered lab access until spring of 2022. In addition, the milli-Kelvin refrigerator necessary to run the experiments stopped working (the prolonged shutdown of the lab was almost certainly a contributing factor) and supply chain issues and lack of original manufacturer technician availability delayed repairs until early 2023.

4. Results

4.1. Characterization of W-Band TKIPs

4.1.1. Experimental Setup: A setup, around a Bluefors cryostat, has been mounted for the characterization of W-band TKIPs (Fig. 1). Unfortunately, after a full diagnostic, it was discovered that the cryostat has a superfluid leak in the dilution unit rendering it operational only down to 4 K. Bluefors has acknowledged the problem and will be replacing the unit soon.

4.1.2. Packaging: JPL designed and fabricated a W-band TKIP. The amplifiers use an inverted microstrip transmission line (Fig. 2a) that has been loaded with capacitive stubs to increase its capacitance. For coupling with the incoming signal, an E-plane probe was used (Fig. 2b). CDL fabricated a waveguide block to mount the amplifiers (Fig. 2c) as schematically shown in Fig. 2d.

(a) (b)

Fig. 1 Experimental setup for characterization of TKPIs amplifiers. (a) Overview of the system. (b) Close up showing feeding waveguides and a packaged parametric amplifier. Due to cooling-power limitations, for W-band characterization, the TKIP has been mounted in the 100 mK stage. In future work, a low-frequency setup will be mounted in the 10-mK stage.

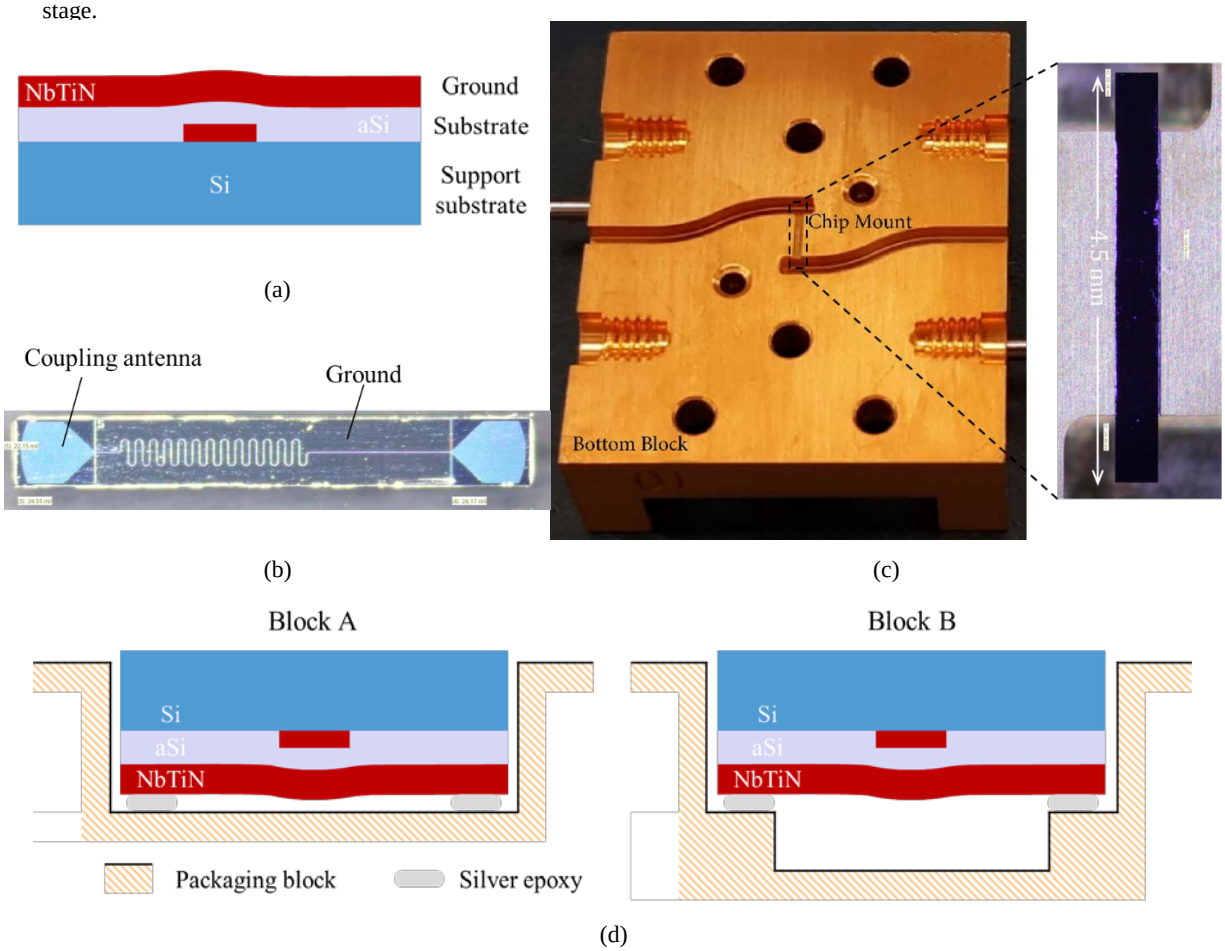

(a) (b) (c) (d)

Fig. 2 Loaded-microstrip TKIPs fabricated at JPL. (a) Schematic of the layered structure used to implement the amplifiers. (b) Top view of the fabricated amplifier. The ground shows a relief produced by the underlying microstrip. (c) Left, bottom part of one of the split blocks used to package the TKIPs. Right, the amplifier is mounted facing down in a channel milled in the block. (d) Schematics of the way the TKIPs are mounted. Left, in block A the mounting channel is flat. Right, in block B an extra slot is milled in the mounting channel.

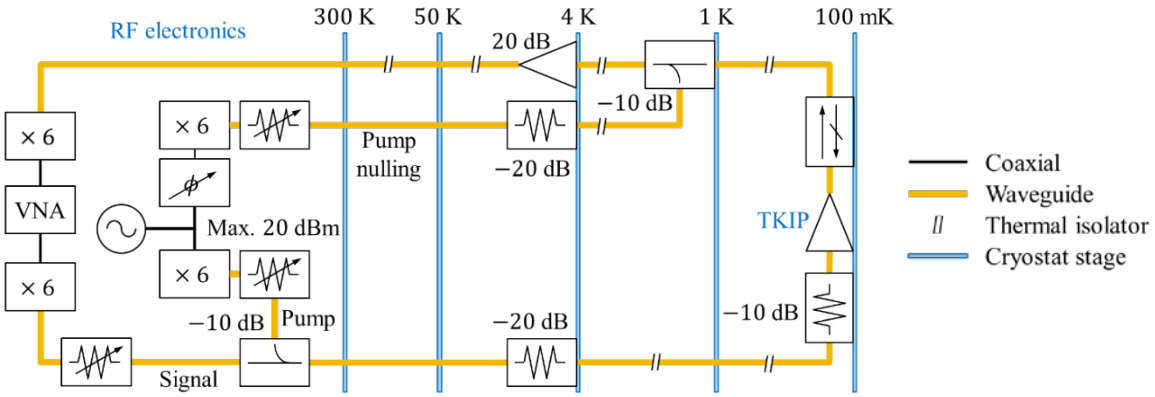

Fig. 3 Layout of the experiment used for gain characterization.

4.1.3. Gain Characterization: Figure 3 shows schematically the setup that was mounted for measuring gain in the parametric amplifiers. The layout is similar to those described in previous works [1]. This implementation uses WR10 waveguides to inject/extract the signals to/from the TKIP mounted in the 100-mK stage. Gap-based thermal isolators [ref] were used reduced the thermal load on the cryostat.

Due to the superfluid leak in the cryostat, only measurements at 4 K were able to be performed. Two TKIPs coming from the same batch from JPL were mounted in two different type of blocks (Fig. 2d) and characterized. Figure 4a shows their transmissions without a pumping frequency. Stopbands are clearly visible at around 100 GHz, according to the design. The fact that both transmissions are of the same order points out to the fact that losses are originated mostly in the amorphous silicon substrate and not to interaction between the TKIP and the mounting block. Figure 4b shows the transmission on the pumped first amplifier. No gain was visible at any pumping frequency and power. In fact, the only effect of increasing the power was to diminish the transmission until, eventually, the device became non-transmitting. These results indicate that the fabricated device has an extremely low critical current produced, probably, by defects on the superconducting strip. Fig. 4c shows the transmission on the pumped second amplifier. In contrast with the first device, a small gain is observed at frequencies above the gap. However, if the power is increased further, the transmission is reduced again and no more gain is observed. Finally, Fig. 4d shows the relative gain of the second amplifier when gain was observed.

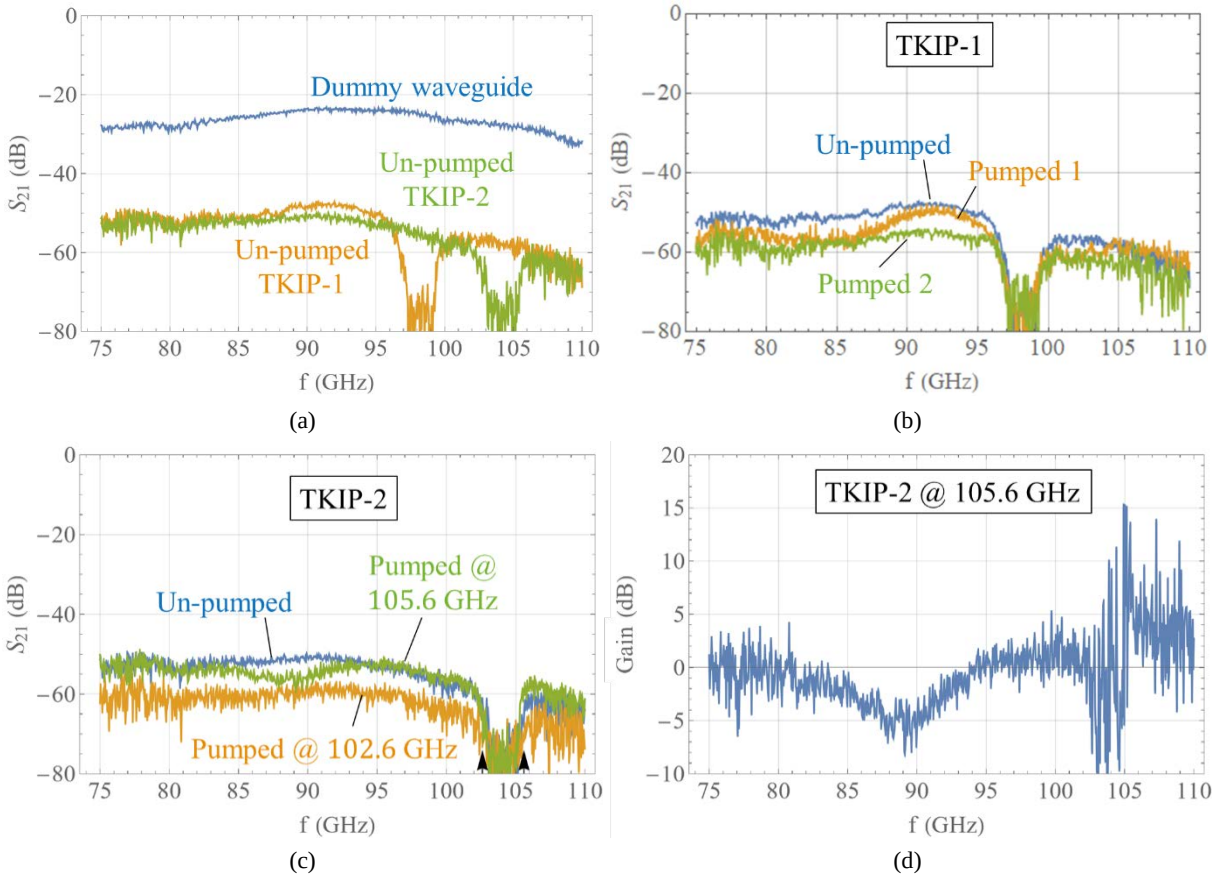

Fig. 4 Gain characterization of two W-band TKIPs. (a) Un-pumped transmission curves of the two devices compared against a dummy waveguide that replaced the TKIPs in the measurement setup. TKIP-1 and TKIP-2 were mounted in blocks type A and B, respectively. (b) Example of pumped transmission curves for TKIP-1. No gain was observed at any pump frequency. (c) Pumped transmission curves for TKIP-2. A small gain was observed at pump frequencies above the designed stopband. Arrows indicate the pump frequencies. (d) Relative gain of TKIP-2 at a pump frequency of 105.6 GHz.

4.1.4. Noise Characterization: The original proposal considered implementing the setup schematically shown in Fig. 5a. The setup is based on state-of-the-art black body loads [2] that, unfortunately, due to pandemics are still not available. As solution, we propose implementing the setup shown in Fig. 5b that has been used successfully to characterize low-noise amplifiers [3]. Most of the components have been acquired for implementation once a working TKIP is achieved.

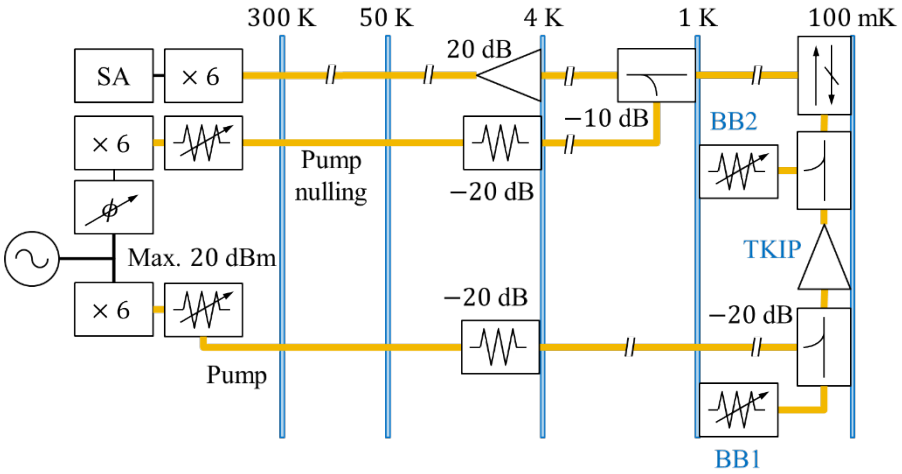

(a)

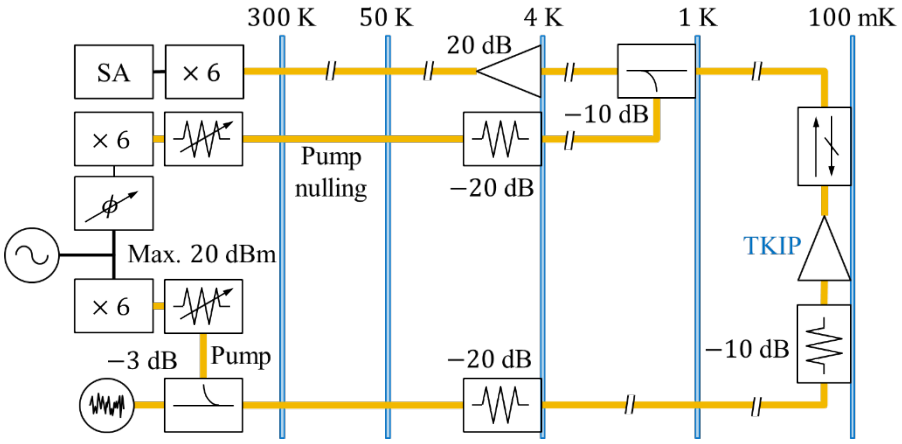

(b)

Fig. 5 Proposed layouts for the noise-characterization characterization experiment. (a) Originally proposed layout. The system is based in 2 temperature-controlled blackbody radiators (BB) that have not been available during the execution of this project. (b) New proposed configuration. Notation is the same as Fig. 3.

4.2. Development of New Techniques at UVML

Wideband TKIPs exploit the purely reactive nonlinear kinetic inductance of a superconducting transmission line to achieve parametric amplification while adding only the noise required by quantum mechanics. To maximize the gain and eliminate other potential sources of noise, one must maximize the phase shift in the transmission line over a practical device footprint while maintaining ultra-low levels of materials-related loss, such as quasi-particle loss inside the superconducting film as a result of high temperature operation (4 K) or loss from two-level-systems inside dielectric materials. Henceforth, at the University of Virginia IFAB, we worked on two fronts:

- Developing growth techniques required for the realization of low-loss NbTiN materials systems
  - Investigating the influence of latticed matched substrates and buffer layers
  - Characterizing thin film thickness uniformity
  - Characterizing NbTiN film properties to allow for accurate TKIP design
- Developing nano-fabrication process to realize TKIPs with a practical footprint

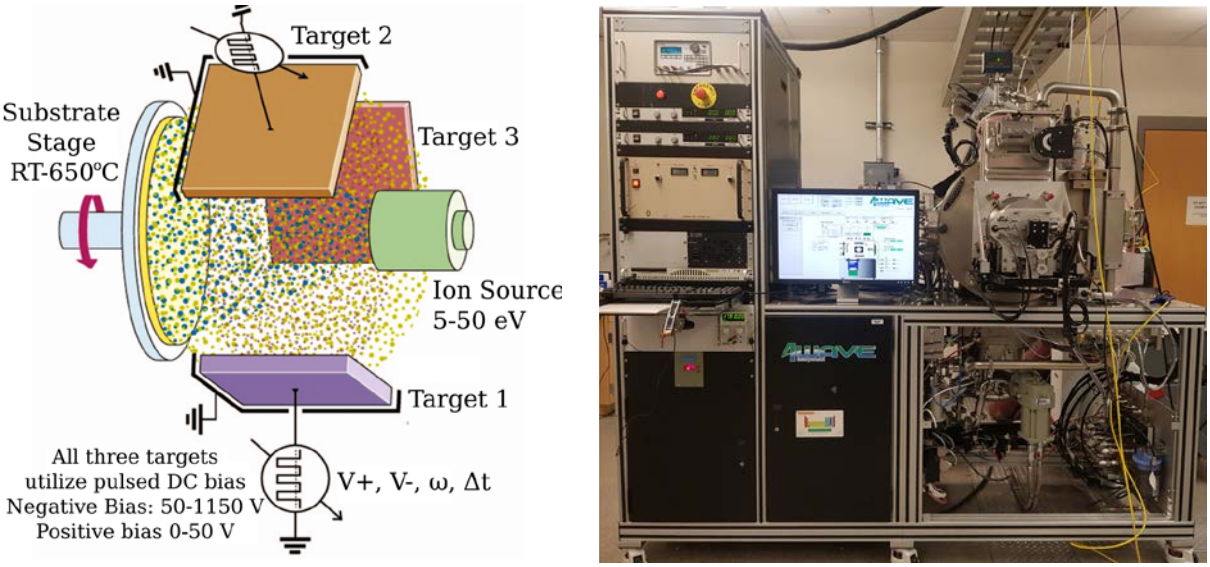

(a) (b)

Fig. 6 (a) Schematic of UVA's 4Wave LANS RBTIBD system. (b) Photograph of the IFAB RBTIBD tool.

- Developing a maskless lithography process
- Switching from Raith150 Two lithography system to a Quantum Design ML3 due to COVID restrictions

4.2.1. Material Growth: We developed a NbTiN thin film deposition process utilizing the IFAB's Reactive Bias Target Ion Beam Deposition (RBTIBD) system shown in Figure 6. RBTIBD is a hybrid between ion beam and conventional magnetron sputter deposition that combines the best of each technique. It uses a low-energy broad beam ion source that reliably produces a controllable density of uniform low-energy (5-50 eV) inert gas ions that cannot re-sputter surface atoms. The flux and dynamics of the incoming ions to the targets are manipulated by independent pulsed DC bias supplies, where the target voltage can be set while the target current is fine-tuned through the pulse width and frequency. Further details of this technology are published elsewhere [4].

a. NbTiN Thickness Uniformity:

TKIPs inherently exploit the nonlinear kinetic inductance of superconducting film to achieve parametric amplification. If we assume the magnetic field only exists within the London penetration depth (λ_L) on the surface of the film, we can define a surface impedance to first order as:

$$Z_S = R_S + jX_S = R_S + j\omega L_S = R_S + j\omega\mu_0\lambda_L \quad (1)$$

However, for film thicknesses on the same order of magnitude as λ_L, magnetic fields can penetrate the film, and the first-order approximation is no longer valid. A more in-depth derivation by Janssen expresses the Z_S of a superconductor as a function of the complex conductivity ($\sigma = \sigma_1 - j\sigma_2$) of the film as:

$$Z_S = R_S + j\omega L_S = \sqrt{\frac{j\omega\mu_0}{\sigma_1 - j\sigma_2}}\coth\left(\frac{t}{\lambda_L}\sqrt{1 + \frac{j\sigma_1}{\sigma_2}}\right) \quad (2)$$

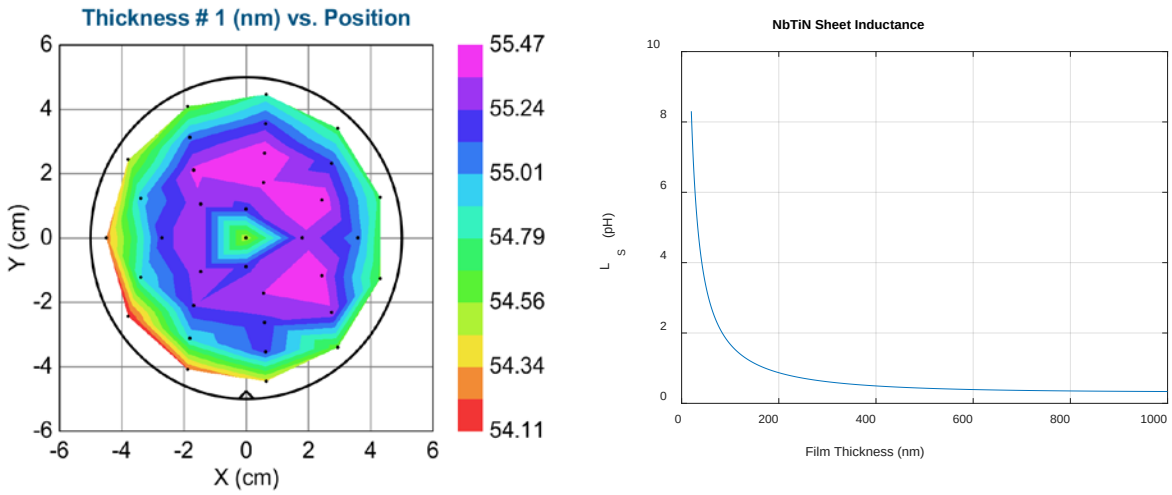

(a) (b)

Fig. 7 (a) Thickness uniformity map of a nominal 50 nm NbTiN film deposited on 4" diameter 100 Si substrate. The average thickness is 54.98 nm with a standard deviation of 0.40 nm, resulting in a thickness uniformity of 0.72% across a 4" substrate. (b) Shown is the variation of L_s as a function NbTiN film thickness, demonstrating the rapid change in L_s for small variations in film thickness when $t \ll \lambda_L$.

where σ is determined by integrating over the density of states using numerical methods [5]. If we assume $T \ll T_C$ and the density of unpaired electrons is insignificant, as is the case for the typical 100 mK operational temperature of TKIP devices, we can estimate the surface impedance as purely reactive. Under these assumptions, one can derive an effective penetration depth (λ_{eff}) and the surface inductance, for a single sided excitation, such as used in micro-strip transmission lines as:

$$L_S = \mu_0 \lambda_{eff} = \mu_0 \lambda_L coth\left(\frac{t}{\lambda_L}\right) \quad (3)$$

Noting the coth(t/λ_L) term, when $t \ll \lambda_L$, L_S is susceptible to small deviations in film thickness and can greatly affect TKIP design parameters. To investigate the variation in NbTiN film thickness, a nominal 50 nm thick NbTiN film was deposited on a 4" diameter 100 Si substrate. NbTiN film thickness was mapped using the IFAB's JA Woollam M-2000 ellipsometer, and the resulting thickness map is shown in Figure 7. The thickness variation was less than 1% across the 4" diameter Si wafer.

b. Electrical properties and TKIP design parameters

Both T_c and resistivity (ρ) of the NbTiN films were measured. From the resistivity, λ_L, and hence kinetic inductance from (3), can be calculated from the empirical relation [6]:

$$\lambda_L(nm) = 105\sqrt{\frac{\rho(\mu\Omega - cm)}{T_C(K)}} \quad (4)$$

Using lattice-matched substrates or buffer layers can enhance the T_c of NbTiN films. In addition, post-deposition annealing can further increase the T_c of RBTIBD NbTiN thin films [7]. In order to investigate both of these effects, 30 nm thick NbTiN films were deposited by room temperature RBTIBD on 100 Si, C-plane sapphire, and 100 Si with a ~100 nm AlN buffer layer. Samples were thermally annealed under a high vacuum at 300° C, the maximum allowable temperature for our fabrication process. Film stress was measured using the wafer deflection technique, the resistivity was measured using the 4-point measurement

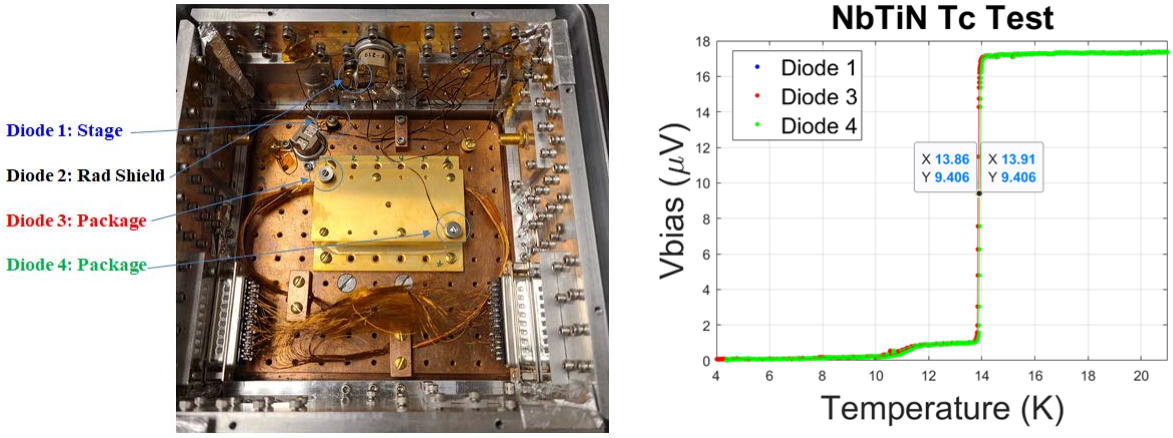

(a) (b)

Fig. 8 (a) View of our closed cycle cryostat showing the 4K stage, 20K radiation shield, test package, and 4 Lakeshore DT-670 diode temperature sensors. The test chip is placed inside the Au-plated test package and connections are made via 4 spring loaded pogo pins. (b) Shown is a typical voltage vs temperature curve of a NbTiN film for a constant 10 microAmp bias. T_c is defined as the average temperature at half the voltage rise.

NbTiN Film Parameters						
Substrate	Annealed	Stress (MPa)	ρ (μΩ-cm)	Tc (K)	λ_L (nm)	Ls (pH)
Si	NA*	-3787	145	11.9	366.52	5.63
Si	300° C	-538	175	13	385.24	6.22
Al2O3	NA*	-1486	140	13	344.57	4.98
Al2O3	300° C	-615	131	14.4	316.69	4.21
Si-AlN	NA*	-1522	142	12.7	351.10	5.17
Si-AlN	300°C	-5388	138	14.9	319.54	4.28

Table 4 Shown are the NbTiN film properties for a 30 nm NbTiN film deposited by RBTIBD. *NA denotes the film properties before thermal annealing.

technique, and Tc was measured using a 4-point measurement system in a closed cycle cryostat shown in Figure 8.

The NbTiN film properties are shown in Table 1. For the case of a pure Si substrate, after thermal annealing, Tc increases from 11.9 to 13.0 K, ρ increases from 145 to 175 μΩ-cm, and stress decreases from -3787 to -538 MPa. Films deposited on sapphire had the highest T_c with comparable stress, but sapphire substrates are incompatible with our fabrication process. Films deposited on Si-AlN demonstrated increased T_c compared to 100 Si substrates, but the film stress is over -5000 GPa after annealing. We note that buckle deformation can occur during fabrication for film stress greater than ~3000 MPa, and are not suitable for this application. NbTiN on Si demonstrates low film stress and increased T_c and ρ after annealing at 300 C and, noting table 3, has the highest kinetic inductance and will be used for TKIP fabrication.

4.2.2. Fabrication: To maximize the nonlinear phase shift, one must realize electrically-long transmission lines containing dispersive engineered structures. Such complex geometries often require sub-micron lithography to realize practical chip geometries. The original scope of this project included developing a sub-micron lithography process using the IFAB's newly purchased Raith150 Two E-beam-Nano Lithography system with an 8 nm beam size. Due to the COVID-19 pandemic and the resulting involuntary lockdowns and restrictions at both NRAO and UVA, the installation and commission of the Raith150 two was delayed and it was not accessible during this project. With this in mind, we modified the project to use

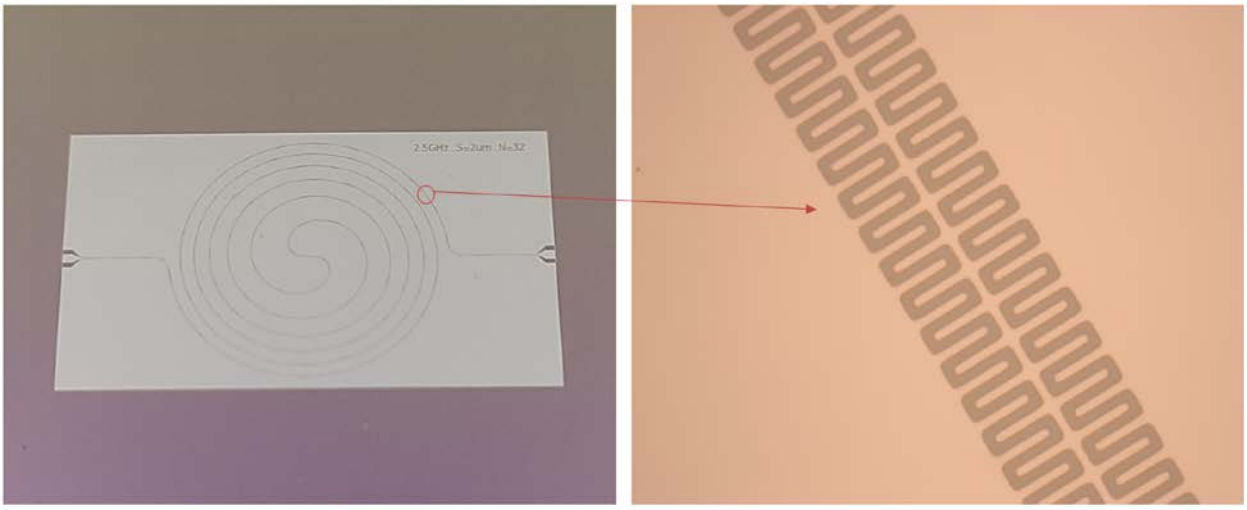

(a) (b)

Fig. 9 (a) Photograph of a 2.5-GHz TKIP pattern realized in 30 nm thick NbTiN on 100 Si substrate. (b) Micrograph showing the detail of the capacitively loaded CPW transmission line with 2.0 μm gap and linewidths.

the IFAB's Quantum Design Microwriter ML3 Direct Lithography System. The ML3 is a maskless projection lithography system utilizing a 385 nm solid-state laser, Digital Mirror Device (DMD), and a series of objective lenses to realize a spot of 400 nm.

Futurrex NR7 250 nm photoresist was used to define capacitively loaded CPW transmission lines with 1.0 and 2.0 um feature sizes. Using these lithography conditions, the pattern of a 2.5 GHz TKIP, designed by Patricio Mena, was transferred to a Si wafer with 30 nm of NbTiN. The NbTiN was subsequently etched using an SF6 chemistry using a Oxford Plasmatherm 100 RIE. An image of the final chip and capacitively loaded CPW line feature defined in a 30 nm NbTiN film is shown in Figure 9.

4.3. Other achievements outside the scope of the original proposal

The new PI has brought new capabilities to NRAO. In parallel to this proposal, he has been working on the modelling and design of TKIPs in different type of implementations. Furthermore, he has also been working on the fabrication and characterization of low-frequency amplifiers. Figure 6 summarizes some of these achievements.

4.3.1. Modelling: The new PI has lead work on extending the amplitude equations as to take into account the complex dispersion and characteristic impedance of the Floquet lines that are commonly used to implement TKIPs [9]. Strong differences with more traditional models have been found. With careful design, larger gains can be found.

4.3.2. Design: The new PI developed an interactive program in Mathematica to ease the design of TKIPs. In order to facilitate the inclusion of more models and make it more accessible to other users, the PI is working with a co-op computer-engineering student in a new version based in Phyton.

4.3.3. Fabrication: A new collaboration with the group of Jochem Baselmans of TU Delft in The Netherlands has been established. Baselmans' group is world-renown for producing state-of-the-art

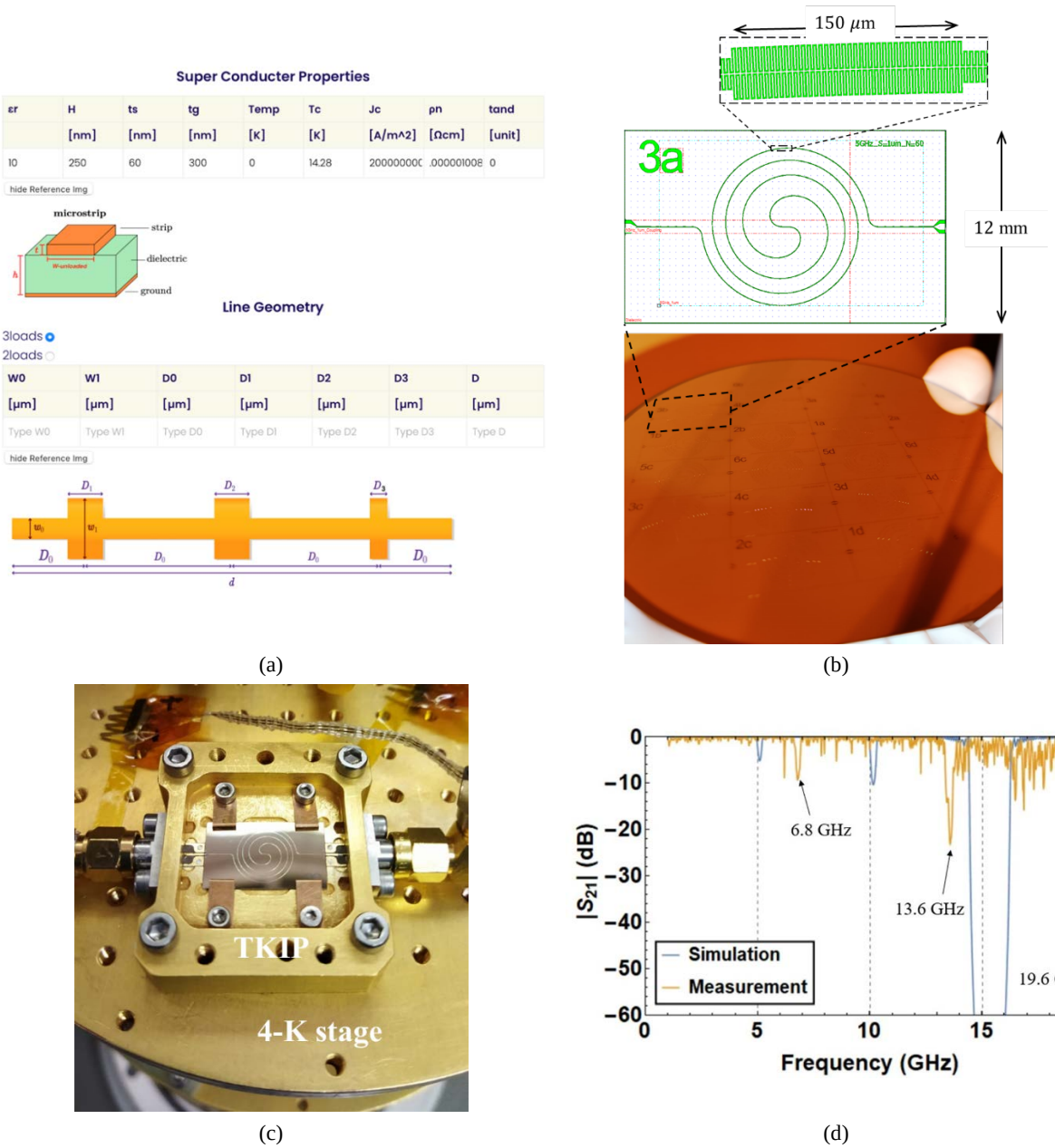

Fig. 6 Other achievements outside the scope of this proposal. (a) Example of the frontend of the interactive tool being developed. (b) Wafer fabricated at TU Delft containing 12 TKIPs implemented using artificial transmission lines. (c) Experimental setup to characterize low-frequency TKIPs mounted in a retrofitted ALMA cartridge. (d) First result showing the transmission of one of the devices. Stopbands are clearly seen at 6.8, 13.6 and 19.6 GHz.

multipixel MKID detectors. These type of detectors also use the kinetic inductance in superconducting films of NbTiNi, the same technology used in TKIPs.

4.3.4. Characterization: A 4-K test setup has been mounted at University of Chile using a retrofitted ALMA cartridge in a testing cryostat. Characterization is undergoing.

5. Conclusions

Accomplishments of this project are:

i. A collaboration with JPL has been established for the development of W-band TKIPs.
ii. A setup for the characterization of W-band TKIPs has been mounted.
iii. Two devices have been characterized. Although transmission shows stopbands as designed, no gain has been measured.
iv. A high-quality NbTiN deposition process has been developed. It has achieved high Tc, >1% thickness variation across a 4" substrate, and high kinetic inductance optimized for the realization of TKIPs.
v. A micron-scale maskless fabrication process was developed, allowing the rapid fabrication of TKIPs in the University of Virginia IFAB.
vi. A new PI has taken lead in the development of TKIPs. He has brought new expertise to CDL.

References

[1] B. Ho Eom, P. Day, H. LeDuc, et al., "A wideband, low-noise superconducting amplifier with high dynamic range," Nature Phys 8, 623–627 (2012). https://doi.org/10.1038/nphys2356.

[2] J. W. Kooi et al., "A Programmable Cryogenic Waveguide Calibration Load With Exceptional Temporal Response and Linearity," in IEEE Transactions on Terahertz Science and Technology, vol. 8, no. 4, pp. 434-445, July 2018, doi: 10.1109/TTHZ.2018.2826838.

[3] J. L. Cano, N. Wadefalk and J. D. Gallego-Puyol, "Ultra-Wideband Chip Attenuator for Precise Noise Measurements at Cryogenic Temperatures," in IEEE Transactions on Microwave Theory and Techniques, vol. 58, no. 9, pp. 2504-2510, Sept. 2010, doi: 10.1109/TMTT.2010.2058276.

[4] M. E. Cyberey, T. Farrahi, J. Lu, R. Weikle, O. Noroozian, and A. W. Lichtenberger, "Growth and characterization of NbTiN films synthesized by reactive bias target ion beam deposition (RBTIBD)," in *Accepted for presentation in 2018 Applied Superconductivity Conference*, Seattle, Washington, Spring 2018.

[5] R. M. J. Janssen, "Multiwavelength observations of active galactic nuclei: Using current facilities and development of enabling technologies," Delft University of Technology, 2017. doi: 10.4233/UUID:8B277229-6A8C-4E8F-942F-9C485DA1E1CE.

[6] T. Matsunaga, H. Maezawa, and T. Noguchi, "Characterization of NbTiN thin films prepared by reactive DC-magnetron sputtering," *IEEE Trans. Appl. Supercond.*, vol. 13, no. 2, pp. 3284–3287, 2003.

[7] T. Farrahi, M. E. Cyberey, M. B. Eller, and A. W. Lichtenberger, "Effect of Post Deposition Annealing on the Structural and Electrical Properties of NbTiN Thin Films Deposited by Reactive Bias Target Ion Beam Deposition Technique," *IEEE Trans. Appl. Supercond.*, pp. 1–1, 2019, doi: 10.1109/TASC.2019.2910024.

[8] T. Farrahi, M. E. Cyberey, M. B. Eller, and A. W. Lichtenberger, "Effect of Post Deposition Annealing on the Structural and Electrical Properties of NbTiN Thin Films Deposited by Reactive Bias Target Ion Beam Deposition Technique," *IEEE Trans. Appl. Supercond.*, pp. 1–1, 2019, doi: 10.1109/TASC.2019.2910024.

[9] J. Carrasco, D. Valenzuela, C. Falcón, R. Finger, and F. P. Mena, "The effect of complex dispersion and characteristic impedance on the gain of superconducting traveling-wave kinetic-inductance parametric amplifiers," *IEEE Trans. Appl. Supercond.*, accepted.